Available online at www.sciencedirect.com
SCIENCE DIRECT®
Journal of Molecular Catalysis A: Chemical 221 (2004) 51–58
JOURNAL OF MOLECULAR CATALYSIS A: CHEMICAL
www.elsevier.com/locate/molcata

Fe-modified $CuMnZrO_2$ catalysts for higher alcohols synthesis from syngas

Run Xu[a], Cheng Yang[a], Wei Wei[a], Wen-huai Li[a], Yu-han Sun[a,*], Tian-dou Hu[b]

[a] *State Key Laboratory of Coal Conversion, Institute of Coal Chemistry, Chinese Academy of Sciences, Taiyuan 030001, PR of China*
[b] *Beijing Synchrotron Radiation Facility, Institute of High Energy Physics, Chinese Academy of Sciences, Beijing 100039, PR of China*

Received 3 February 2004; received in revised form 26 May 2004; accepted 1 July 2004
Available online 14 August 2004

Abstract

The effect of iron on the structural and catalytic properties of $CuMnZrO_2$ catalysts used for higher alcohols synthesis has been investigated by several techniques (BET, X-ray diffraction (XRD), extended X-ray absorption fine structure (EXAFS), temperature program reduction (TPR), CO-FTIR and CO hydrogenation). It was found that the presence of iron resulted in substantial changes in both structure properties and catalytic performance. The copper dispersion increased and the catalyst stabilization was improved. The role of iron was dependent on the method of catalyst preparation. The co-precipitation method produced highly dispersed copper species, which favored the synthesis of methanol and branched alcohols. However, the wetness impregnation method gave rise to highly dispersed copper and copper–iron phase, which showed a good performance for synthesis of straight-chain alcohols. Such differences in the performance of catalysts could be attributed to the extent of iron oxide-support interaction, which led to the presence of metallic iron phases in the reduced catalyst.

Keywords: $CuMnZrO_2$ catalyst; Iron promoter; Preparation method; Higher alcohols synthesis

1. Introduction

In the last 30 years, much attention has been paid to synthesis of higher alcohols from coal or natural gas via syngas due to its potential application as a good gasoline blend or alternative motor fuel for the reduction of exhaust emission. As a result, several catalytic systems for higher alcohol synthesis through CO hydrogenation were developed.

Generally, the catalysts for higher alcohol synthesis fall into two broad categories [1–3]: one is to produce methanol and branched alcohols (i.e. isobutanol), such as alkali-promoted $Cu/ZnO/Al_2O_3$ catalysts [4–6]; the other is to form straight-chain alcohols, such as molybdenum sulfide type catalysts [1] and Co/Cu-based catalysts [3,7–9]. The straight-chain products followed a Schulz–Flory type distribution. The catalyst system based on the $Co–Cu/ZnO/Al_2O_3$ catalysts has received the most attention on terms of basic research [8,10,11]. The Fischer–Tropsch elements were used because of their strong ability to promote carbon chain growth [12]. The principle that underlies the development of these catalysts is the combination of a methanol synthesis function provided by the copper, and a chain growth function provided by the Fischer–Tropsch elements for that the cobalt and iron were most commonly used. The incorporation of cobalt or iron phases in a multi-component catalyst resulted in substantial changes in both activity and product distributions.

In our previous work, $CuMnZrO_2$ catalyst showed the high activity and selectivity for synthesis of methanol, which was modified by Fischer–Tropsch elements (Fe, Co, Ni) to develop the catalysts for high alcohols synthesis [13]. Among them, the presence of iron greatly enhanced the formation of higher alcohols, which were a mixture of straight chain alcohols and branched alcohols (mainly isobutanol). Furthermore, the performance of iron-modified $CuMnZrO_2$ catalyst was considered dependent on the

* Corresponding author. Tel.: +86 3514049612; fax: +86 3514041153.
E-mail address: yhsun@sxicc.ac.cn (Y.-h. Sun).

1381-1169/$ – see front matter © 2004 Elsevier B.V. All rights reserved.
doi:10.1016/j.molcata.2004.07.003

catalyst preparation method [14]. In the present work, the role of iron in multi-component Fe–$CuMnZrO_2$ catalysts was explored by comparison of binary and ternary catalysts, while co-precipitation and wetness impregnation methods were used to prepare the Fe–$CuMnZrO_2$ catalysts for higher alcohols synthesis to understand the effect of iron introduction on the carbon chain growth.

2. Experimental

2.1. Catalysts preparation

The binary and ternary catalysts were prepared by co-precipitation of a solution of copper, manganese, iron nitrates (one or two of them) and $ZrOCl_2{\cdot}8H_2O$ with an aqueous solution of Na_2CO_3 at 343 K and a constant pH of 10 in a well-stirred thermo-stated container. Then the precipitates were aged at 343 K for 2 h. Afterward the precipitates were washed thoroughly with distilled water, and were dried at 393 K for 12 h and then calcined at 623 K in air for 3 h.

The iron-modified $CuMnZrO_2$ catalysts were prepared by two methods. Fe–$CuMnZrO_2$(C) was prepared using the same procedures as for $CuMnZrO_2$, except that $Fe(NO_3)_3{\cdot}9H_2O$ was introduced into the mixed solutions. Fe–$CuMnZrO_2$(I) was prepared by wetness impregnation method on the $CuMnZrO_2$ catalyst with $Fe(NO_3)_3$ aqueous solution. The composition of the catalysts were as follows: Cu:Mn:Zr:Fe = 1:0.5:2:0.1 (molar ratio). It was also determined by ICP emission spectrometry.

2.2. Characterization methods

The BET surface areas of the catalysts were determined by N_2 adsorption at 77 K using the Tristar 3000 Chemical Adsorption Instrument (Micromeritics). Powder X-ray diffraction (XRD) patterns were recorded on a Rigaku D/Max diffractorments with a Cu target and Ni filter.

X-ray adsorption spectra around the Cu K-adsorption edge were obtained using the deamline of 4W1B of Beijing Synchrotron Radiation Facility (BSRF). The storage ring was operated at 2.2 GeV with a typical current of 50 mA. The fixed-exit Si (1 1 1) flat double crystals were used as monochromator. The extended X-ray absorption fine structure (EXAFS) data were processed with the National Synchrotron Radiation Laboratory analysis programs (NSRLXAFS). A total of 4.0 nearest oxygen was found for each copper site at an average distance of 0.195 nm on the bulk CuO and these results were in good agreement with the conclusion of crystal analysis, which indicated that the fixed error in our experimentation and data analysis was very low.

Temperature program reduction (TPR) was carried out in a U-tube quartz reactor with a hydrogen–argon mixture (containing 5 vol.% of hydrogen) as the reductive gas. The samples (50 mg) were flushed with an argon flow of 50 $cm^3\ min^{-1}$ at 393 K to remove water and then reduced in a flow of H_2+Ar at a rate of 10 K min^{-1} with a programmable temperature controller. Hydrogen consumption was monitored by a thermal conductivity cell (TCD) attached to a gas chromatograph (GC-950). The effluent gas was passed through a cold trap placed before TCD in order to remove water from the exit stream of the reactor. The hydrogen consumption of various catalysts was calculated on the basis of the area of their TPR profiles and the profile of the standard sample of CuO.

The diffuse reflectance FTIR (DRIFT) spectra were recorded using Nicolet Magna-II 550 FTIR spectrometer equipped with spectra-tech diffuse reflectance accessory and a high temperature in situ cell with ZnSe windows. A KBr beam splitter has been used with a TGS detector. The catalyst was reduced in situ for 6 h under atmospheric pressure by a stream of H_2 at 573 K and was treated with a flushing gas. Subsequently, the system was cooled down to 298 K. After introduction of CO (99.995%) for 1 h, the catalyst surface was purged with argon (99.99%) to remove gaseous CO and then IR spectra were recorded.

2.3. Catalytic test

The activity tests were conducted with a fixed-bed, stainless flow micro reactor. All catalysts were reduced in a hydrogen–nitrogen mixture (containing 5 vol.% of hydrogen) flow at 573 K and atmospheric pressure before syngas exposure. The steady-state activity measurements were taken after at least 48 h on the stream. The analysis of the gaseous and liquid products was made by Shimazu-8A gas chromatographs. Thermal conductivity detector equipped with a TDX-101 column determined H_2, CO, CH_4 and CO_2. The water and methanol in liquids were also detected by TCD with a GDX-401 column. The alcohols and hydrocarbons were analyzed by flame ionization detector (FID) with a Propake-Q column.

3. Results and discussion

3.1. Texture and structure of catalysts

As listed in Table 1, the BET surface area of the $CuZrO_2$ catalyst was 61 $m^2\ g^{-1}$ with the mean pore radius of 4.2 nm. The addition of iron caused greatly increase of the surface area, while the mean pore radius decreased. This result indicated that the interaction between iron and zirconia occurred. $CuMnZrO_2$ catalyst showed large surface area, 193 $m^2\ g^{-1}$, with the mean pore radius of 3.3 nm (see Fig. 1). The addi-

Table 1
Texture parameters of various catalysts

Sample	S_{BET} ($m^2\ g^{-1}$)	r_P (nm)	V_P ($mL\ g^{-1}$)
$CuZrO_2$	61	4.2	0.06
Fe–$CuZrO_2$	112	2.7	0.08
$CuMnZrO_2$	193	3.3	0.16
Fe–$CuMnZrO_2$(C)	197	4.0	0.20
Fe–$CuMnZrO_2$(I)	86	6.7	0.14

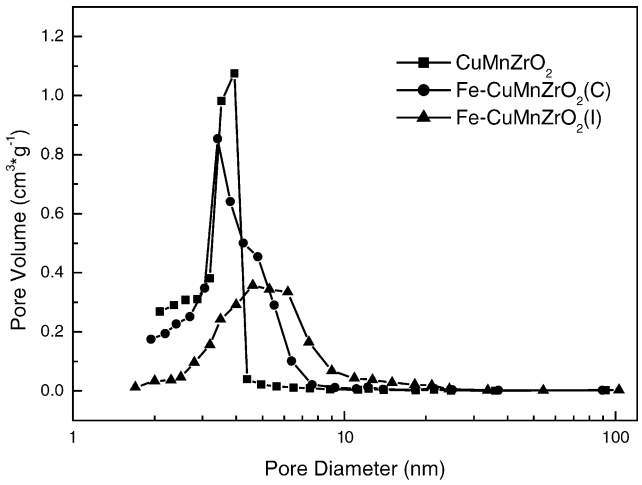

Fig. 1. Pore size distribution of various catalysts.

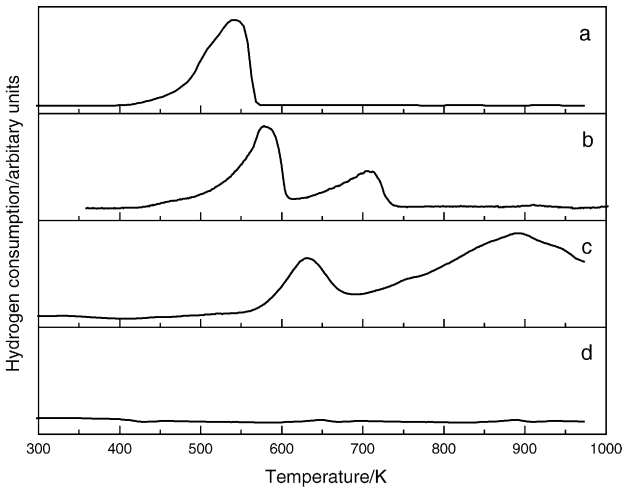

Fig. 2. TPR profiles of pure metal oxides: (a) CuO; (b) MnO_2; (c) Fe_2O_3; (d) ZrO_2.

tion of iron could enlarge pore radius of Fe–$CuMnZrO_2$(C) and Fe–$CuMnZrO_2$(I) up to 4.0 and 6.7 nm, respectively. But the surface area of Fe–$CuMnZrO_2$(I) drastically decreased to 86 $m^2\ g^{-1}$.

Iron-modified catalysts, similar to $CuZrO_2$ and $CuMnZrO_2$, hardly showed the obvious XRD patterns, suggesting that the components were highly dispersed on the amorphous zirconia surface. Extended X-ray absorption fine structure provided an obvious difference between them (see Table 2). The introduction of iron had obviously influenced on the CuO coordination surrounding. The copper coordination number for $CuZrO_2$ decreased with the addition of iron. This revealed that when iron was introduced, the copper species existed in much smaller crystallites and exhibited an amorphous-like or less well-ordered structure feature. Compared to $CuMnZrO_2$ catalyst, the copper coordination number for Fe–$CuMnZrO_2$(C) catalyst decreased and the distance of Cu–O increased. This change was more obviously for the Fe–$CuMnZrO_2$(I) catalyst. The high Debye–Waller factors associated with this shell also indicated the copper presented great disorder. Therefore, the interaction between copper and iron in Fe–$CuMnZrO_2$(I) was stronger than that in Fe–$CuMnZrO_2$(C).

3.2. Temperature program reduction of the catalysts

The TPR curves of pure metal oxides were shown in Fig. 2. for comparison. CuO was more reducible than other metal oxides. Hematite (α-Fe_2O_3) showed two H_2 consumption peaks, a smaller one at 630 K corresponding to the reduction of Fe_2O_3 to Fe_3O_4 and a larger asymmetric peak at higher temperature (895 K) due to Fe^{3+} reduction to Fe^{2+} and then to metallic iron [15]. For MnO_2 sample, two peaks were observed at 559 and 653 K, this result was ascribed to the stepwise reduction sequence: $MnO_2 \rightarrow Mn_3O_4 \rightarrow MnO$ [16]. The

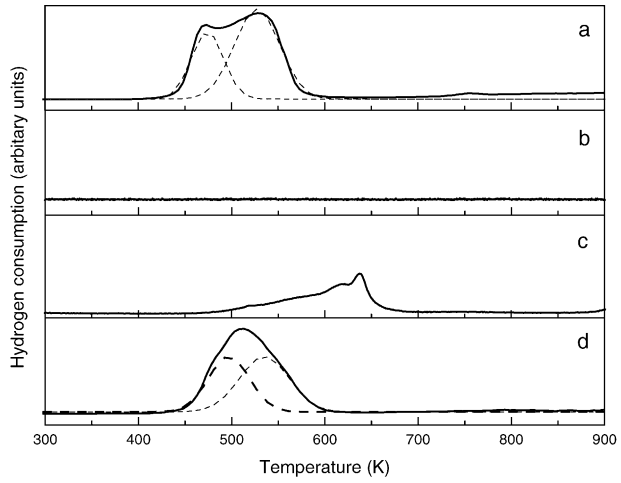

Fig. 3. TPR profiles of binary and ternary catalysts: (a) $CuZrO_2$; (b) $FeZrO_2$; (c) $MnZrO_2$; (d) Fe–$CuZrO_2$.

Table 2
Fitting results of CuO EXAFS for Cu—O band

Sample	Shell	Coordination number	Shell radius (nm)	Debye–Waller factors (10^{-4} nm^2)
CuO	Cu—O	4.00	0.195	–
$CuZrO_2$	Cu—O	3.77	0.194	0.21
Fe–$CuZrO_2$	Cu—O	3.73	0.195	0.25
$CuMnZrO_2$	Cu—O	3.62	0.197	0.44
Fe–$CuMnZrO_2$(C)	Cu—O	3.50	0.198	0.51
Fe–$CuMnZrO_2$(I)	Cu—O	3.19	0.199	0.63

Note: Fitting range in κ-space: 2.0–10.0 $Å^{-1}$ with the weight of κ^3.

Table 3
Hydrogen consumption of various catalysts from the integration area of TPR profiles

Sample	H_2 consumption (mmol g^{-1})	Degree of reduction[a] (%)
$CuZrO_2$	3.07	98.05
$MnZrO_2$	0.71	41.4
$FeZrO_2$	–	–
Fe–$CuZrO_2$	3.10	97.23
$CuMnZrO_2$	3.52	86.70
Fe–$CuMnZrO_2$(C)	3.50	85.16
Fe–$CuMnZrO_2$(I)	3.61	87.10

[a] The degree of reduction was calculated on the basis of their H_2 consumption in experiments and the amount for the reduction of maximum valence metal oxide to metal.

ZrO_2 sample did not show any distinct reduction peak, suggesting the ZrO_2 was hardly reducible at present condition.

Temperature program reduction profiles of binary and ternary catalysts were displayed in Fig. 3. The H_2 consumption for the reduction of catalysts was summarized in Table 3. Two peaks of H_2 consumption were observed at 503 and 523 K for $CuZrO_2$ catalyst, corresponding to the reduction of highly dispersed CuO and the reduction of bulk CuO [17,18], respectively. Moreover, the H_2 consumption was very close to the value necessary for the reduction of CuO, which indicated complete reduction of CuO to metallic Cu. For $MnZrO_2$ catalyst, a wide and asymmetric peak was detected at 640 K. Koh et al. [19] investigated Mn–Zr oxide catalysts prepared by co-precipitation and found that manganese oxide was composed a mixture of Mn_3O_4 and Mn_2O_3 after calcination in air at 773 K. Moreover, several researches [20,21] indicated manganese was present in calcined catalysts at least partly as Mn^{2+}. Wilson et al. [22] have reported that Mn^{2+} could not be reduced to the metallic state. Therefore, the TPR peak for our $MnZrO_2$ catalyst was ascribed to the reduction of mixture oxide (Mn^{4+} and Mn^{3+}) to Mn^{2+}. Obviously, the H_2 consumption was less than the amount for the reduction of MnO_2 to MnO, suggesting that the manganese was present in catalysts as mixture oxide. The $FeZrO_2$ catalyst did not show any distinct reduction peak. It was possible that the amount of Fe was too small to be detected or the interaction between Fe and ZrO_2 was too strong to reduce at present condition.

When Fe was introduced in $CuZrO_2$, the TPR peaks shifted to higher temperature and exhibited a higher intensity of the peak of lower temperature at the expense of the magnitude of higher temperature one. The results indicated that the addition of iron led to an increase in the dispersion of copper and the interaction of the copper with other components was enhanced. Moreover, the H_2 consumption of Fe–$CuZrO_2$ slightly decreased compared with $CuZrO_2$, suggesting the iron inhibited the reduction of CuO.

The presence of Mn greatly influenced the reduction of $CuZrO_2$ catalyst (see Fig. 4). The first peak corresponding to the reduction of highly dispersed CuO increased obviously

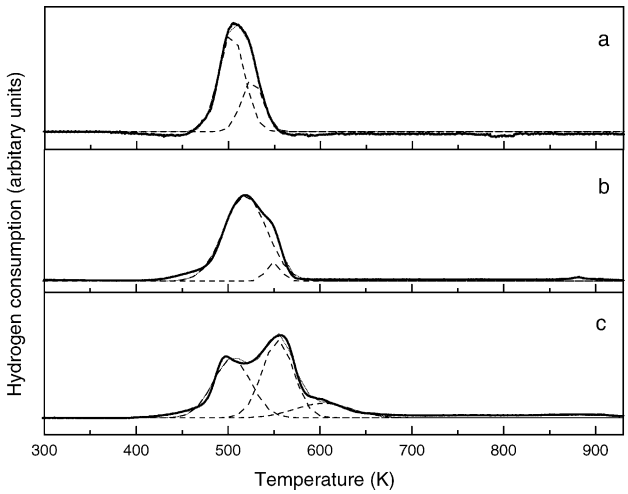

Fig. 4. TPR profiles of iron-modified catalysts: (a) $CuMnZrO_2$; (b) Fe–$CuMnZrO_2$(C); (c) Fe–$CuMnZrO_2$(I).

and the second peak corresponding to the reduction of bulk CuO became to a little shoulder. It was noteworthy that the overall H_2 consumption (3.52 mmol g^{-1}) was less than the total H_2 consumption amount for the reduction of $CuZrO_2$ (3.07 mmol g^{-1}) plus $MnZrO_2$ (0.71 mmol g^{-1}). This indicated that there might be some CuO that cannot be completely reduced to metallic Cu due to its interaction with manganese oxides [23].

The Fe–$CuMnZrO_2$(C) also showed two H_2 consumption peaks, while they obviously shifted to higher temperature (see Fig. 4) compared with $CuMnZrO_2$. The peak of low temperature was predominant, implying that iron enhanced the dispersion of CuO. The total H_2 consumption for Fe–$CuMnZrO_2$(C), 3.50 mmol g^{-1}, was similar to the $CuMnZrO_2$, suggested that the iron was hardly reduced. Fe–$CuMnZrO_2$(I) showed three reduction peaks at 504, 554 and 604 K, respectively. The peak at 504 K, similar to that on $CuMnZrO_2$, should be ascribed to the reduction of highly dispersed CuO species. The peak at 554 K should be ascribed to the reduction of CuO species, which had an interaction with iron. It could not be ascribed to bulk CuO because the presence of iron in the Fe–$CuMnZrO_2$(I) played a key role in increase the dispersion of copper as pointed out in the section on EXAFS (see Table 2). The higher temperature peak should be ascribed to the reduction of bulk CuO or manganese oxides. Furthermore, the H_2 consumption for Fe–$CuMnZrO_2$(I), 3.61 mmol g^{-1}, was higher than that of $CuMnZrO_2$, implying that some Fe^{3+} was reduced. On the one hand, the reduction of iron oxide was strongly influenced by the preparation method and then the extent of iron oxide-support interaction. Iron oxide was reduced over 773 K in co-precipitation $FeZrO_2$ catalyst [24], while it could be reduced at 673 K in a Fe/ZrO_2 catalyst prepared by impregnation method [25,26]. Baker and coworkers also found that the reduction of cobalt was rather difficult in co-precipitated catalysts than that in impregnation catalysts for the cobalt-modified Cu/ZnO/Al_2O_3 system due to different

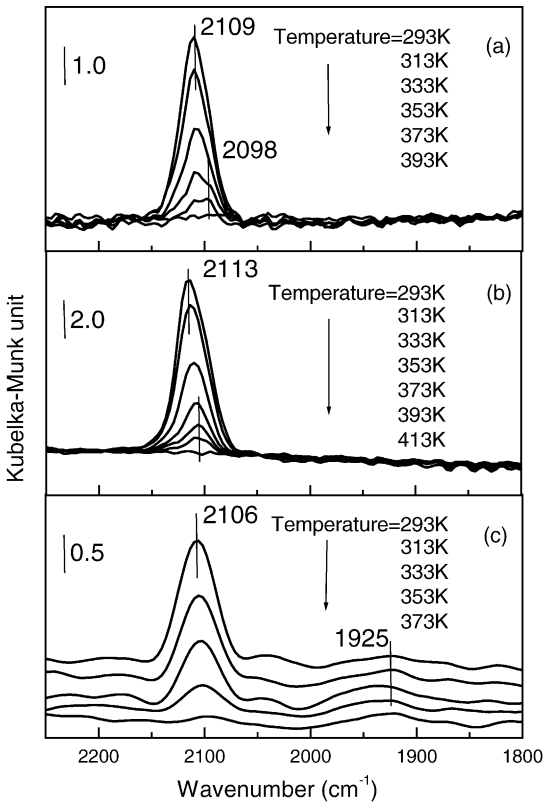

Fig. 5. FTIR spectra of CO adsorbed on the catalysts: (a) $CuMnZrO_2$; (b) Fe–$CuMnZrO_2$(C); (c) Fe–$CuMnZrO_2$(I).

degree of metal-support interaction [27]. On the other hand, the interaction between copper and iron should inhibited the reduction of CuO, while the reduction of iron species became easier due to the active hydrogen spilling-over from the reduced Cu particles. Therefore, the iron coupled with copper to form a kind of active phase in Fe–$CuMnZrO_2$(I) catalyst.

3.3. Diffuse reflectance FTIR spectra

Fig. 5 gives the FTIR spectra obtained after CO adsorption on various catalysts. When CO adsorption on $CuMnZrO_2$ catalysts carried out at 298 K, only a single band evolved at about 2109 cm^{-1} (see Fig. 5a), which decreased with the rise of temperature. With the temperature up to 333 K two adsorption bands appeared at 2109 and 2098 cm^{-1}, corresponding to linear CO species on different copper sites [28]. The band at 2109 cm^{-1} was caused by the formation of adsorbed CO on highly dispersed copper sites, and the band at 2098 cm^{-1} was assigned to the species formed on densely packed surface [29,30]. This result was in the agreement with the findings of TPR study, which indicated the copper oxide was present in highly dispersed CuO and bulk CuO.

Compared with $CuMnZrO_2$, the adsorption of CO on Fe–$CuMnZrO_2$(C) showed one strong band at 2113 cm^{-1} (see Fig. 5b), corresponding to the linearly adsorbed CO on highly dispersed copper site, which showed a red shift with the rise of temperature. This indicated that a kind of homogeneous copper site formed on the surface due to the addition of iron. However, the band intensity of adsorbed CO on Fe–$CuMnZrO_2$(I) was very weak, which was partially due to the low surface area (see Fig. 5c). Two distinct bands appeared at 2106 and 1925 cm^{-1}, which were attributed to the linear CO species on highly dispersed copper particles and bridge-form species on Fe^0 particles [28,31]. These results suggested that iron acted as structural promoter in Fe–$CuMnZrO_2$(C), which increased copper dispersion, while the iron was partially reduced and plausibly coupled with copper to form a kind of active phase in Fe–$CuMnZrO_2$(I) catalyst.

3.4. CO hydrogenation over the catalysts

The $CuZrO_2$ catalyst showed a high activity and selectivity for methanol synthesis under mild reaction condition

Table 4
The catalytic performance for CO hydrogenation over various catalysts

Catalysts	Reaction Temperature (K)	CO conversion (%)	Carbon selectivity[a] (%)			Alcohols yield ($g\,mL^{-1}\,h^{-1}$)	C_2^+OH in alcohols (wt.%)
			CO_2	HC[b]	ROH		
$CuZrO_2$	523	28.3	11.0	6.1	82.8	0.38	1.5
	563	13.1	14.1	36.7	49.1	0.21	1.8
Fe–$CuZrO_2$	563	7.8	9.7	22.6	66.7	0.19	4.9
	573	13.6	10.5	23.6	65.9	0.23	7.2
$CuMnZrO_2$	553	26.5	3.9	6.3	89.8	0.82	2.3
	563	33.5	12.6	9.8	77.6	0.92	4.1
	573	37.3	18.0	17.9	64.1	0.85	6.0
Fe–$CuMnZrO_2$(C)	563	21.9	26.7	41.5	31.8	0.28	15.1
	573	29.4	27.7	43.2	29.1	0.34	18.5
	583	38.3	33.8	46.8	19.4	0.42	18.9
Fe–$CuMnZrO_2$(I)	563	26.0	34.6	37.6	27.8	0.25	22.6
	573	36.6	32.7	37.6	29.7	0.36	24.4
	583	45.5	33.2	40.6	26.2	0.45	25.2

Reaction conditions: 8.0 MPa, 8000 h^{-1}, H_2/CO = 2.0.

[a] Selectivity based on number of atoms per gram carbon = [number of CO converted to given product/total number of CO converted] × 100%.

[b] HC: Hydrocarbons.

[32]. However, it could be found that with the rise of reaction temperature, the catalyst activity and the selectivity of alcohols decreased (see Table 4). This was due to the sinter of Cu on the surface [33]. The presence of iron greatly influenced the performance of the $CuZrO_2$ catalyst. The content of higher alcohols in the liquid products slightly increased, while the higher hydrocarbon in the outlet gas increased, too. Moreover, the catalyst showed good performance in the stabilization.

The $CuMnZrO_2$ catalyst showed the high activity and selectivity towards methanol synthesis with the maximum at 563 K. The tendency for methanation and other hydrocarbon formation increased as the temperature was increased. The alcohol production was favored at low temperature, whereas a little proportion of higher alcohols produced at high temperature. For the Fe–$CuMnZrO_2$(C) catalyst, overall activity was suppressed and the total alcohol selectivity greatly decreased compared to $CuMnZrO_2$ catalyst, while the carbon selectivity to CO_2 was increased as well as the selectivity to hydrocarbons. However, the suppression of hydrogenation activity by iron would allow partially hydrogenated CH_x species to remain for longer periods, and these were involved in the C–C chain formation leading to the production of higher alcohols and hydrocarbons. The carbon chain growth was noticeably observed over Fe–$CuMnZrO_2$(C) catalyst and the proportion of $C_2{}^+$ alcohols in total alcohols increased up to more than 15%. The trend in the overall activity coupled with the trend in space-time yield increased quickly with the rise of reaction temperature. However, both CO_2 and hydrocarbons selectivity increased, while the total alcohols selectivity decreased with the rise of temperature. For the Fe–$CuMnZrO_2$(I) catalyst, the higher alcohols fraction represented 22.5% of the total alcohol production and it increased to 25.2% with the increase of temperature, while the space-time yield reached 0.45 g mL^{-1} h^{-1}. It was interesting that the Fe–$CuMnZrO_2$(I) showed good performance in the stabilization compared to $CuMnZrO_2$ and Fe–$CuMnZrO_2$(C). The total alcohol selectivity only slightly decreased with the rise of temperature.

For $CuMnZrO_2$, the formation of methanol reduced with the rise of CO conversion (see Fig. 6a). The higher alcohols were produced in relatively small amounts and tended to increase slightly in amount with the increasing CO conversion. The ethanol was predominant in $C_2{}^+$OH. For the Fe–$CuMnZrO_2$(C) catalyst, the increasing CO conversion clearly favored the formation of the butanol (mainly isobutanol) but not other alcohols (see Fig. 6b). This indicated that the Fe–$CuMnZrO_2$(C) had a character, which resembled alkali-modified methanol catalyst, because the formation of branched products [4,6] was a characteristic feature of alkali-modified Cu catalysts under alcohols synthesis conditions.

It was noteworthy that the Fe–$CuMnZrO_2$(I) showed different properties. Increasing CO conversion favored the formation of the linear alcohols, such as ethanol, propanol (see Fig. 6c). Only a little isobutanol could be detected. The absence of branched products demonstrated that the copper component in the catalyst was profoundly modified by iron. It suggested that the role of the iron in alcohols synthesis could be ascribed to the interaction with copper, which gave the active sites for carbon chain growth [34].

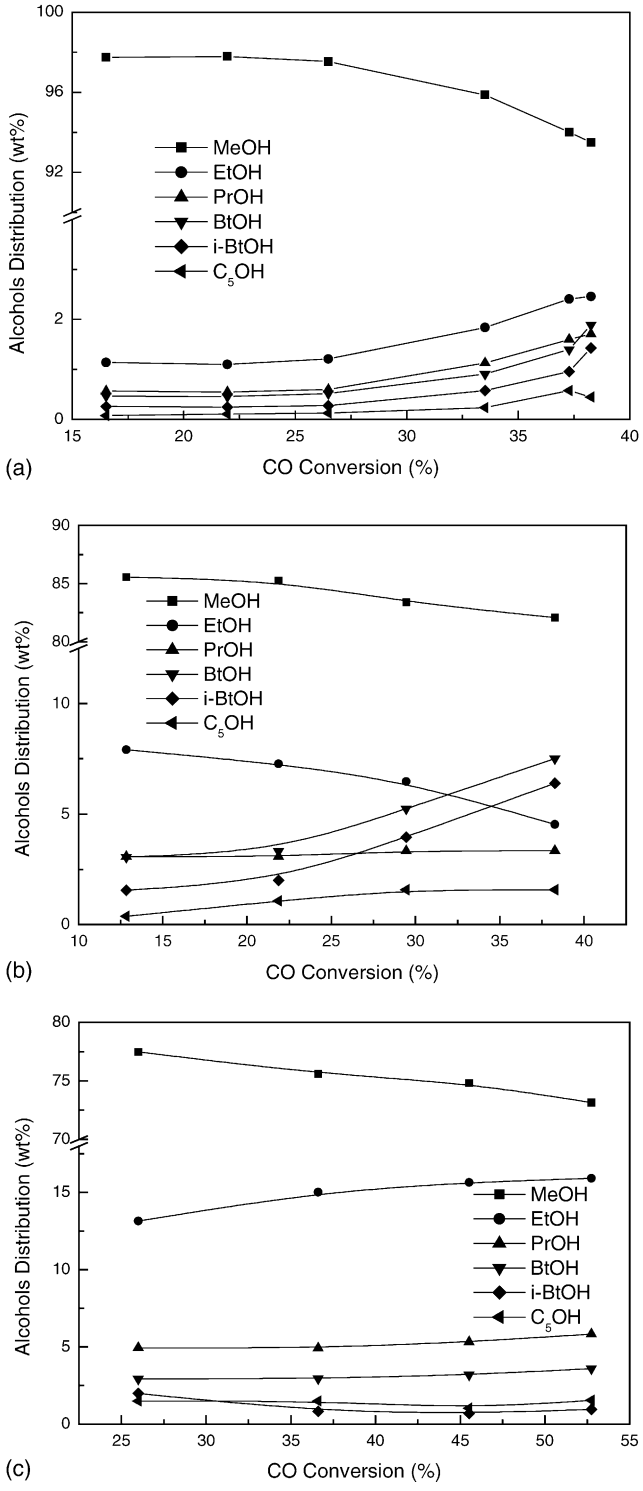

Fig. 6. The change of alcohols distribution with the CO conversion over the catalysts: (a) $CuMnZrO_2$; (b) Fe–$CuMnZrO_2$(C); (c) Fe–$CuMnZrO_2$(I).

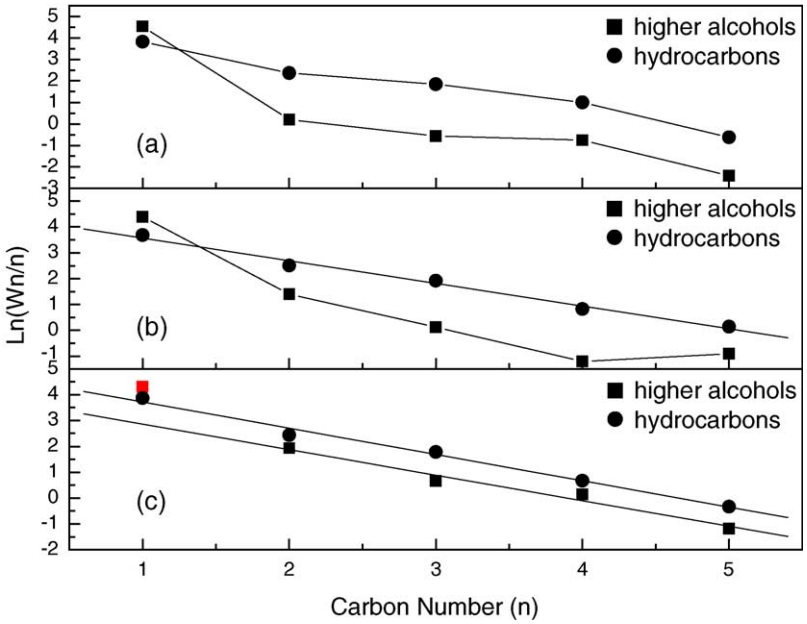

Fig. 7. The Schulz–Flory plot of linear alcohols and hydrocarbons products on catalysts. Reaction condition: 583 K, 8.0 MPa, 8000 h^{-1} (a) $CuMnZrO_2$; (b) Fe–$CuMnZrO_2$(C); (c) Fe–$CuMnZrO_2$(I).

With regard to product distributions patterns, both higher alcohols and hydrocarbons were not in line with the Schulz–Flory distribution for $CuMnZrO_2$ (see Fig. 7a). The alcohols formation was not in line with the Schulz–Flory distribution for the Fe–$CuMnZrO_2$(C), but the hydrocarbons distribution followed the Schulz–Flory equation very well (see Fig. 7b), suggesting that the formation of hydrocarbons and alcohols was in different active sites. Thus, it could be suggested that the hydrocarbons was produced on iron sites and the alcohols was produced on copper sites. There was little interaction between iron and copper sites. The higher alcohols might come from aldol condensation reactions.

For the Fe–$CuMnZrO_2$(I) catalyst, we found a chain propagation factor of 0.37 ± 0.02 for higher alcohols and 0.36 ± 0.02 for higher hydrocarbons (see Fig. 7c). The rate of methanol formation was not in line with higher alcohols according to the Schulz–Flory distribution, which was higher than expected. Thus, the production of methanol was suggested to take place at different active sites from the higher alcohols synthesis sites. Furthermore, the chain propagation factor for hydrocarbons was practically same as that for higher alcohols. This could be taken as further indirect evidence that the hydrocarbons and higher alcohols come from the same active sites. Therefore, the reaction of hydroxycarbene and carbene species forming higher alcohol precursors was the major chain-growth step and the attachment of CH_x species occurred on the last carbon so that no branched alcohols and hydrocarbons were observed.

4. Conclusion

The role of iron elements in multi-component Fe–$CuMnZrO_2$ catalysts was explored by comparison of binary and ternary catalysts, while co-precipitation and wetness impregnation methods were used to prepare the Fe–$CuMnZrO_2$ catalysts for higher alcohols synthesis to understand the effect of iron introduction on the carbon chain growth. The incorporation of iron promoter resulted in substantial changes in both structure properties and catalytic performance. The dispersion of copper increased and the catalyst stabilization was improved. Moreover, the effect of iron was greatly influenced by catalyst preparation methods. It was found that for the catalyst prepared by co-precipitation method, iron species acted as structural promoter, which increased copper dispersion and improved the formation the homogeneous copper phase. As a result, the introduction of iron by co-precipitation method was favorable to synthesis of methanol and branched products. For the catalyst prepared by wetness impregnation method, the iron oxide-support interaction was relatively weak. The iron oxide could be partially reduced, which led to increase of the interaction between highly dispersed copper and iron. Such interaction was in favor of chain growth to form higher alcohols.

Acknowledgment

This work was supported by the State Key Foundation Project for Development and Research of China (G1999022400) and Knowledge Innovation Program of Chinese Academy of Sciences (KGCX2-302).

References

[1] X. Xu, E.B.M. Doesburg, J.J.F. Scholten, Catal. Today 2 (1987) 125.
[2] P. Forzatti, E. Tronconi, I. Pasquon, Catal. Rev. Sci. Eng. 33 (1991) 109.

[3] J.A. Dalmon, P. Chaumette, C. Mirodatos, Catal. Today 15 (1992) 101.
[4] K.J. Smith, R.B. Anderson, J. Catal. 85 (1984) 428.
[5] J.M. Camposmartin, A. Guerreroruiz, J.L.G. Fierro, J. Catal. 156 (1995) 208.
[6] I. Boz, M. Sahibzada, I.S. Metcalfe, Ind. Eng. Chem. Res. 33 (1994) 2021.
[7] A. Sugier, E. Freund, US Patent 4122110 (1978).
[8] P. Courty, D. Durand, E. Freund, A. Sugier, J. Mol. Catal. 17 (1982) 241.
[9] G.R. Sheffer, R.A. Jacobson, T.S. King, J. Catal. 116 (1989) 95.
[10] A. Kiennemann, C. Diagne, J.P. Hindermann, P. Chaumette, P. Courty, Appl. Catal. 53 (1989) 197.
[11] W.M.H. Sachtler, Proceedings of the eighth International Congress on Catalysis, Berlin,1984, Verlag Chemie, Weinheim, 1984, p. 152.
[12] I. Boz, Catal. Lett. 87 (2003) 187.
[13] N. Zhao, R. Xu, W. Wei, Y.H. Sun, React. Kinet. Catal. Lett. 75 (2002) 297.
[14] R. Xu, Z. Ma, C. Yang, W. Wei, Y. Sun, Prepr. Am. Chem. Soc., Div. Fuel Chem. 48 (2003) 217.
[15] P.A. Webb, C. Orr, Analytical Methods in Fine Particle Technology, Micromeritics Instrument Corporation, Norcross, GA, USA, 1997 (p. 265).
[16] H. Trevino, G.D. Lei, W.M.H. Sachtler, J. Catal. 154 (1995) 245.
[17] M. Shimokawabe, H. Asakawa, N. Takezawa, Appl. Catal. 59 (1990) 45.
[18] R. Zhou, T. Yu, X. Jiang, F. Chen, X. Zheng, Appl. Surf. Sci. 148 (1999) 263.
[19] D.J. Koh, J.S. Chung, Y.G. Kim, J.S. Lee, I. Nam, S.H. Moon, J. Catal. 138 (1992) 630.
[20] A. Wöllner, F. Lange, H. Schmelz, H. Knözinger, Appl. Catal. A 94 (1993) 181.
[21] M. Kilo, J. Weigel, A. Wokaun, R.A. Koeppel, A. Stoeckli, A. Baiker, J. Mol. Catal. A 126 (1997) 169.
[22] T.P. Wilson, P.H. Kasai, P.C. Ellgen, J. Catal. 69 (1981) 193.
[23] Y. Tanaka, T. Utaka, R. Kikuchi, T. Takeguchi, K. Sasaki, K. Eguchi, J. Catal. 215 (2003) 271.
[24] A.F.H. Wielers, A.J.H.M. Kock, C.E.C.A. Hop, J.W. Geus, A.M. van Der Kraan, J. Catal. 117 (1989) 1.
[25] J.-J. Huang, J.R. Anderson, J. Catal. 40 (1975) 143.
[26] E. Guglielminotti, J. Phys. Chem. 98 (1994) 4884.
[27] J.E. Baker, R. Burch, S.E. Golunski, Appl. Catal. 53 (1989) 279.
[28] .P. Hollins, J. Pritchard, Vibrational spectroscopies for adsorbed species, in: A.T. Bell, M.L. Hair (Eds.), ACS Symposium Series, American Chemical Society, Washington, D.C., 1979, p. 51.
[29] F. Boccuzi, A. Chiorino, G. Martra, M. Gargano, N. Ravasio, B. Carrozzini, J. Catal. 165 (1997) 129.
[30] A.R. Balkenende, C.J.G. van Des Grift, E.A. Meulenkamp, J.W. Geus, Appl. Surf. Sci. 68 (1993) 161.
[31] N. Sheppard, T.T. Nguyen, Advances in Infrared and Raman Spectroscopy, 1978 (p. 67).
[32] Y.H. Sun, P.A. Sermon, J. Chem. Soc. Chem. Commun. (1993) 1242.
[33] Y.H. Sun, P.A. Sermon, Catal. Lett. 29 (1994) 361.
[34] A. Kiennemann, A. Barama, S. Boujana, M.M. Bettahar, Appl. Catal. A 99 (1993) 175.